Simulation on Greenberger–Horne–Zeilinger (GHZ) state under Markovian Z-type Dephasing

Brandon Liu

November 20, 2025

Abstract

Greenberger–Horne–Zeilinger (GHZ) states are highly sensitive to phase noise because their global coherence resides entirely in the off-diagonal element $\left|0^{\otimes N}\right\rangle\left\langle 1^{\otimes N}\right|$. In this report I study memoryless (Markovian) Z-type dephasing that acts only during explicit waits in a simple circuit model. I sweep GHZ sizes $N \in \{3, 4, 5\}$, the total circuit depth d, and a *repeats* parameter controlling the number of idle identity gates per qubit per wait layer. I track two figures (i) state fidelity with the ideal GHZ projector and (ii) logarithmic negativity across the $1|(N-1)$ bipartition. Using Qiskit Aer's density-matrix simulator, I compare the numerical results to a closed-form dephasing model, map the phase-damping probability to a physical T_2 time, and briefly contrast pure dephasing with amplitude damping and depolarising noise. Both metrics show monotonic degradation with depth and size, and the analytic model agrees with the simulation within numerical precision across the parameter range considered.

1 Introduction

Multipartite GHZ states

$$|\mathrm{GHZ}_N\rangle = \frac{1}{\sqrt{2}}\left(|0\rangle^{\otimes N} + |1\rangle^{\otimes N}\right) \tag{1}$$

are a standard probe of quantum coherence and entanglement. Their global coherence is concentrated entirely in the off-diagonal element $\left|0^{\otimes N}\right\rangle\left\langle 1^{\otimes N}\right|$, which makes them extremely fragile under phase noise. Understanding how this coherence decays under realistic noise models is relevant for near-term quantum devices, where idle periods and dephasing dominate many error budgets.

In this report I focus on a simple scenario: GHZ states exposed to memoryless Z-type dephasing that acts only during explicit wait periods in the circuit. Using Qiskit Aer's density-matrix backend, I simulate circuits that

1. prepare an N-qubit GHZ state,
2. insert a sequence of wait layers built from single-qubit identity gates,
3. attach Markovian phase-damping channels only to these identity gates.

I then sweep over the number of wait layers and a *repeats* parameter controlling how many idle identity gates are applied per qubit per layer. For each configuration I compute the fidelity to the ideal GHZ state and the logarithmic negativity across the $1|(N-1)$ cut.

Beyond raw plots, I used a compact analytic model for the GHZ coherence under this noise, show that it matches the simulated fidelity curves, reinterpret the phase-damping probability in terms of a physical T_2 time, and compare pure dephasing with other Markovian channels.

2 Theory

2.1 GHZ states and dephasing

The pure GHZ density matrix is

$$\rho_{\mathrm{GHZ}} = |\mathrm{GHZ}_N\rangle\langle\mathrm{GHZ}_N| = \frac{1}{2}\Big(\big|0^{\otimes N}\big\rangle\big\langle 0^{\otimes N}\big| + \big|1^{\otimes N}\big\rangle\big\langle 1^{\otimes N}\big| + \big|0^{\otimes N}\big\rangle\big\langle 1^{\otimes N}\big| + \big|1^{\otimes N}\big\rangle\big\langle 0^{\otimes N}\big|\Big). \quad (2)$$

Under Z-type dephasing, the populations $\big|0^{\otimes N}\big\rangle\big\langle 0^{\otimes N}\big|$ and $\big|1^{\otimes N}\big\rangle\big\langle 1^{\otimes N}\big|$ are preserved, while the off-diagonal terms are exponentially suppressed.

A single-qubit phase-damping channel with parameter λ has Kraus operators

$$K_0 = \sqrt{1-\lambda}\, I, \qquad K_1 = \sqrt{\lambda}\, |0\rangle\langle 0|\,, \qquad K_2 = \sqrt{\lambda}\, |1\rangle\langle 1|\,. \quad (3)$$

Applied to a single qubit, this channel leaves the populations invariant and multiplies the off-diagonal elements by a coherence factor

$$c = \sqrt{1-\lambda}. \quad (4)$$

For an N-qubit GHZ state, independent phase-damping on each qubit multiplies the global coherence $\big|0^{\otimes N}\big\rangle\big\langle 1^{\otimes N}\big|$ by c^N per application of the channel.

2.2 Time-based view and T_2

For a Markovian pure dephasing process with characteristic time T_2, a single qubit undergoing a wait of duration Δt experiences

$$c = e^{-\Delta t/T_2}, \quad (5)$$

so that the off-diagonal elements decay as e^{-t/T_2} and the populations are unchanged. Relating this to the Kraus representation,

$$\lambda = 1 - c^2 = 1 - e^{-2\Delta t/T_2}, \quad (6)$$

so the phase-damping probability used in the simulator can be interpreted directly in terms of T_2 and the chosen time step Δt

2.3 Circuit model and depth-based dephasing

In the circuits considered here, depth is defined as follows:

- depth $d = 1$ consists of a single preparation layer that creates the GHZ state from $|0\rangle^{\otimes N}$ using one Hadamard and $N-1$ CNOTs;
- each additional depth step adds one *wait layer* built from identity gates.

Let r denote the number of identity "wait" gates per qubit per wait layer. For total depth d there are $(d-1)$ wait layers, so each qubit sees

$$\text{hits per qubit} = r(d-1) \quad (7)$$

applications of the phase-damping channel. Assuming:

- independent, Markovian dephasing on each qubit,
- no noise on the GHZ preparation gates,

the GHZ coherence decays as

$$\gamma(d) = c^{Nr(d-1)}. \quad (8)$$

2.4 Fidelity

Because the GHZ state lives in the two-dimensional subspace spanned by $\{|0^{\otimes N}\rangle, |1^{\otimes N}\rangle\}$ and the populations are preserved, the fidelity of the decohered state $\rho(d)$ with the ideal GHZ state is [1]

$$F(d) = \langle \mathrm{GHZ}_N | \, \rho(d) \, | \mathrm{GHZ}_N \rangle = \frac{1}{2}\big(1 + \gamma(d)\big) = \frac{1}{2}\big(1 + c^{Nr(d-1)}\big). \tag{9}$$

2.5 Logarithmic negativity

To quantify entanglement across the $1|(N-1)$ bipartition, I use the logarithmic negativity [4], which is based on the positive partial transpose (PPT) criterion [2, 3]:

$$\mathcal{E}_N(\rho) = \log_2 \big\| \rho^{T_A} \big\|_1, \tag{10}$$

where T_A denotes the partial transpose on the first qubit and $\| \cdot \|_1$ is the trace norm.

3 Methods

3.1 Simulation backend and noise model

All simulations are performed using Qiskit Aer's `density_matrix` simulator, so Kraus channels are applied exactly and there is no stochastic sampling noise [5]. To ensure that wait layers are preserved as intended, I transpile with optimisation level 0 and restrict the basis gates to `['id']` (plus the gates used for GHZ preparation).

3.2 Parameter sweeps

Unless otherwise stated, I sweep:

- GHZ sizes $N \in \{3, 4, 5\}$,
- depths $d = 1, \ldots, 16$,
- per-wait dephasing probability $p_{\mathrm{phase}} = \lambda = 0.02$,
- repeats $r = 1$ (with additional plots exploring $r > 1$).

For each $(N, d, r, p_{\mathrm{phase}})$ I build the corresponding circuit, run a single density-matrix simulation, and post-process the resulting $\rho(d)$.

3.3 Metrics and implementation details

The two main metrics are:

1. *State fidelity*
$$F(d) = \langle \mathrm{GHZ}_N | \, \rho(d) \, | \mathrm{GHZ}_N \rangle \, , \tag{11}$$
computed using Qiskit's `state_fidelity` between the simulated density matrix and the ideal GHZ projector.

2. *Logarithmic negativity* across the $1|(N-1)$ cut,
$$\mathcal{E}_N(d) = \log_2 \big\| \rho^{T_A}(d) \big\|_1. \tag{12}$$
Numerically, I rearrange the density matrix indices to implement the partial transpose on the first qubit and compute the trace norm using a singular value decomposition.

4 Results and Discussion

4.1 Fidelity versus circuit depth

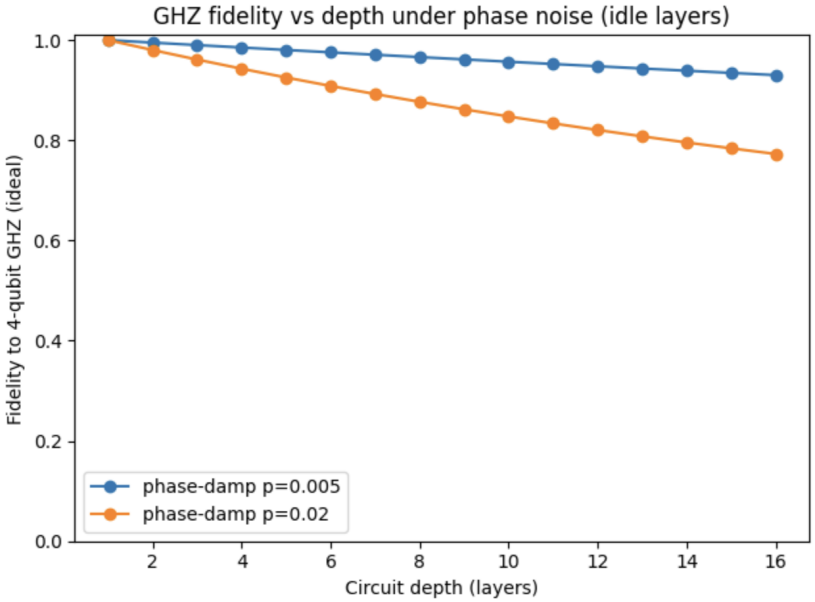

Figure 4.1: Fidelity to GHZ_n vs. circuit depth for $n = 4$ under idle-only Z-type dephasing (defaults p_{phase}, r, and depth range as in Methods).

Figure 4.1 reports the state fidelity

4.2 Effect of repeats (idle ticks) on fidelity

I vary the number of identity "ticks" per wait layer, denoted by repeats r, while keeping n and p_{phase} fixed. Increasing r exposes each qubit to more dephasing hits per depth step. As expected, the fidelity curve steepens with larger r, and the gap between traces widens as depth increases.

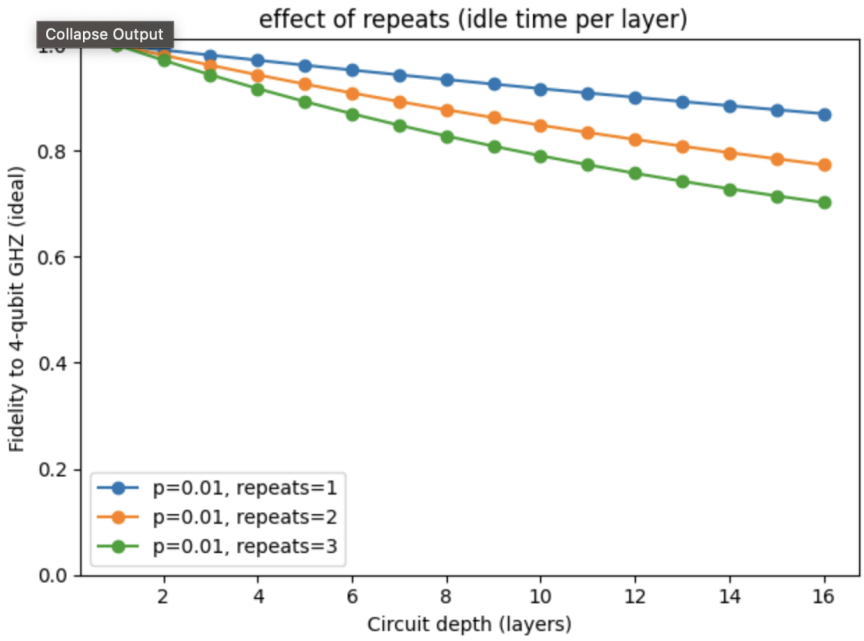

Figure 4.2: Effect of repeats r on fidelity vs. depth (example: $n = 4$, $p_{\text{phase}} = 0.02$). Larger r (more idle ticks per wait layer) yields a steeper decay.

4.3 Size dependence ($n = 3, 4, 5$)

Figure 4.3 compares $F(d)$ directly across sizes. The ordering $F_{n=3}(d) \geq F_{n=4}(d) \geq F_{n=5}(d)$ holds for all depths shown, and the separation grows with d. This illustrates the size sensitivity of GHZ coherence to Z-type dephasing.

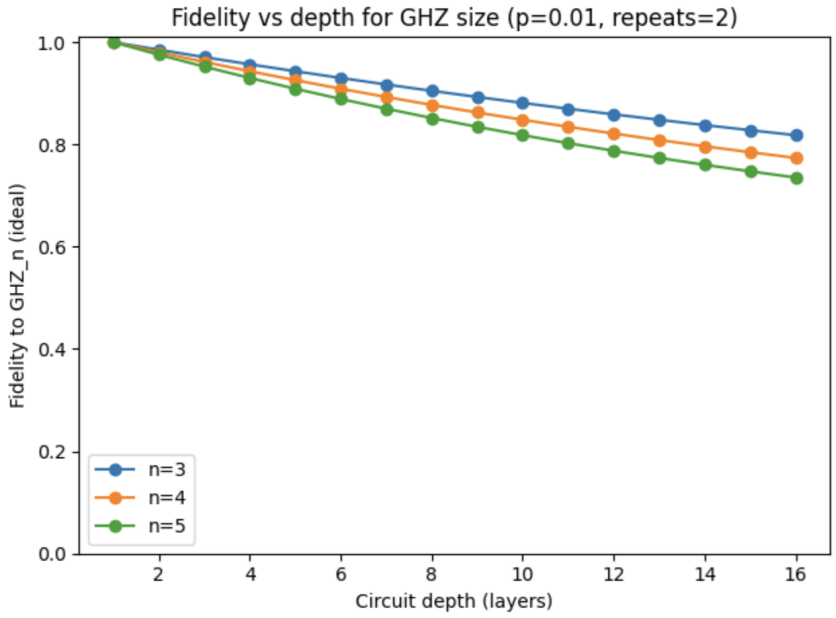

Figure 4.3: Fidelity vs. depth for $n \in \{3, 4, 5\}$. Larger GHZ states lose coherence faster under the same per-wait dephasing.

Taken together, Figs. 4.1–4.3 show a consistent picture of how fidelity behaves under idle-only Z-type dephasing up to depth $d = 16$:

- **Monotonic trend.** For each GHZ size n and repeats r, the fidelity $F(\rho) = \langle \mathrm{GHZ}_N|\rho|\mathrm{GHZ}_N\rangle$ decreases monotonically with depth. At $d = 1$ (no waits) I observe $F \simeq 1$, and then a gradual drop as wait layers are added.
- **Size ordering.** Across depths, the traces satisfy $F_{n=3}(d) \geq F_{n=4}(d) \geq F_{n=5}(d)$, reflecting the fact that more qubits experience the same per-wait dephasing in parallel (Fig. 4.1 vs. Fig. 4.2).
- **Repeats effect.** Increasing the number of identity ticks per wait layer (repeats r) steepens the decay at fixed n and noise strength (Fig. 4.3). Each depth step then accumulates more dephasing hits.

These qualitative features follow from the standard phase-damping model. A single wait "hit" has coherence factor

$$c = \sqrt{1-\lambda},$$

so with n qubits, repeats r, and depth d (one preparation layer plus $d-1$ waits) the global GHZ coherence is

$$\gamma(d) = c^{\,n\,r\,(d-1)}.$$

Because the prepared state occupies the $\{|0^N\rangle, |1^N\rangle\}$ subspace, the fidelity trace is

$$F(d) = \tfrac{1}{2}\big(1+\gamma(d)\big) = \tfrac{1}{2}\Big(1 + c^{\,n\,r\,(d-1)}\Big).$$

Two practical remarks for the depth range plotted: (i) within $d \leq 16$ and the noise strengths used, the curves do *not* visibly approach the $F = \frac{1}{2}$ floor—this is expected when $c \lesssim 1$ (small λ), since many depth steps are required to halve the coherence; (ii) the per-depth multiplicative factor is c^{nr}, so a semilog view of $2F(d) - 1$ would appear approximately linear:

$$\log\big(2F(d)-1\big) = (d-1)\,n\,r\,\log c,$$

with slope set by nr and $\log c < 0$. This linearization explains the clear separation between sizes in Fig. 4.1/4.2 and the separation between repeat settings in Fig. 4.3 over the finite depth window shown.

4.4 Logarithmic negativity versus circuit depth (Fig. 4.4)

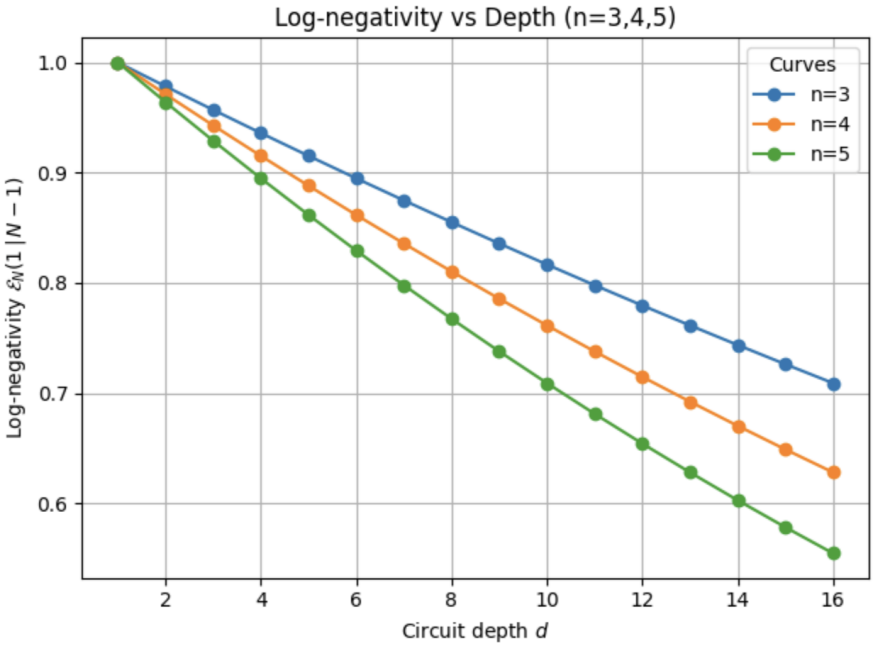

Figure 4.4: Logarithmic negativity $\mathcal{E}_N(1\,|\,N{-}1)$ vs. depth for $n \in \{3, 4, 5\}$. Entanglement decreases monotonically with depth and with system size.

Figure 4.4 shows the logarithmic negativity across the $1\,|\,(N{-}1)$ cut,

$$\mathcal{E}_N(\rho) = \log_2 \left\| \rho^{T_A} \right\|_1,$$

as a function of depth d under idle-only Z-type dephasing. The trends across Figs. 4.1–4.3 carry over here:

- **Monotonic decay within the plotted window.** $\mathcal{E}_N$ starts near 1 bit at $d = 1$ (prepared GHZ) and decreases with d; within $d \leq 16$ it remains clearly above 0 (no sudden entanglement death at these noise levels).
- **Size ordering and repeats.** For fixed depth, $\mathcal{E}_N$ satisfies $\mathcal{E}_{N=3} \geq \mathcal{E}_{N=4} \geq \mathcal{E}_{N=5}$, and larger repeats r (more idle ticks per layer) reduce $\mathcal{E}_N$ faster—mirroring the fidelity ordering in Figs. 4.1–4.3.
- **Curvature.** Because $\log_2(1 + x)$ is concave, differences are compressed when coherence is high (near $d = 1$) and spread out as depth increases.

Under memoryless, wait-only dephasing the negativity follows the GHZ coherence $\gamma(d)$:

$$\mathcal{E}_N(d) = \log_2\big(1 + \gamma(d)\big), \qquad \gamma(d) = c^{\,n\,r\,(d-1)}, \qquad c = \sqrt{1-\lambda}.$$

Equivalently, as long as the state fidelity satisfies $F(d) \geq \frac{1}{2}$ in the plotted range,

$$\mathcal{E}_N(d) = \log_2\big(2F(d)\big),$$

so the ranking of curves with n and r matches that seen in the fidelity figures. Practically, for $d \leq 16$ and the noise strengths used here, $\mathcal{E}_N$ decays visibly but does not approach 0, consistent with the limited depth window and small per-wait dephasing.

4.5 Numeric vs analytic fidelity

Using the analytic model for $\gamma(d)$, I compute the closed-form fidelity $F_{\text{th}}(d) = \frac{1}{2}(1 + \gamma(d))$ and overlay it with the Qiskit data. Across all tested sizes and depths, the numeric fidelity points lie on top of the analytic curves to graphical precision. On a semi-logarithmic plot of $2F(d) - 1$ vs d, the decay appears approximately linear with slope $Nr \log c < 0$, as expected from the $c^{Nr(d-1)}$ dependence. This agreement confirms that the phase-damping channel and circuit construction implement the intended Markovian dephasing model.

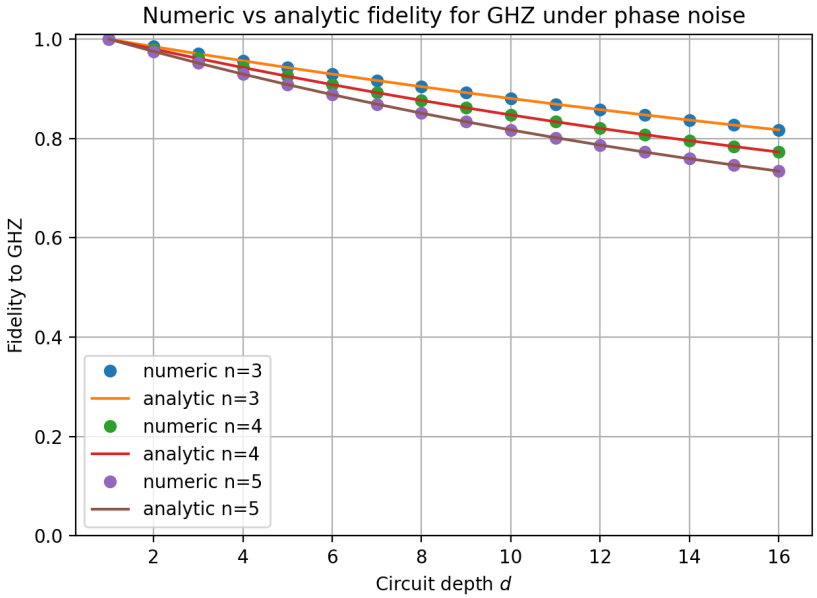

Figure 4.5: GHZ fidelity as a function of circuit depth d for $N = 3, 4, 5$ under three different single-qubit noise channels applied to idle `id` gates: pure phase damping (dephasing), amplitude damping, and single-qubit depolarising noise. All channels use the same nominal error probability $p = 0.02$. Pure dephasing preserves populations and suppresses only coherence, amplitude damping drives the state towards $|0\rangle^{\otimes N}$, and depolarising noise drives it towards the maximally mixed state, leading to distinct fidelity decay profiles for the GHZ state.

4.6 Mapping depth to physical time and T_2

To connect depth to a physical decoherence time, I interpret each wait layer as a fixed time step Δt and use

$$c = e^{-\Delta t/T_2}, \qquad \lambda = 1 - c^2 = 1 - e^{-2\Delta t/T_2} \tag{13}$$

to choose $p_{\text{phase}} = \lambda$ for a given T_2 and Δt. For example, with $T_2 = 50\,\mu\text{s}$ and $\Delta t = 5\,\mu\text{s}$, the derived p_{phase} yields fidelity curves $F(t)$ that again coincide with the analytic expression

$$\gamma(t) = e^{-Nt/T_2}, \qquad F(t) = \frac{1 + \gamma(t)}{2}, \qquad t = (d-1)r\Delta t. \tag{14}$$

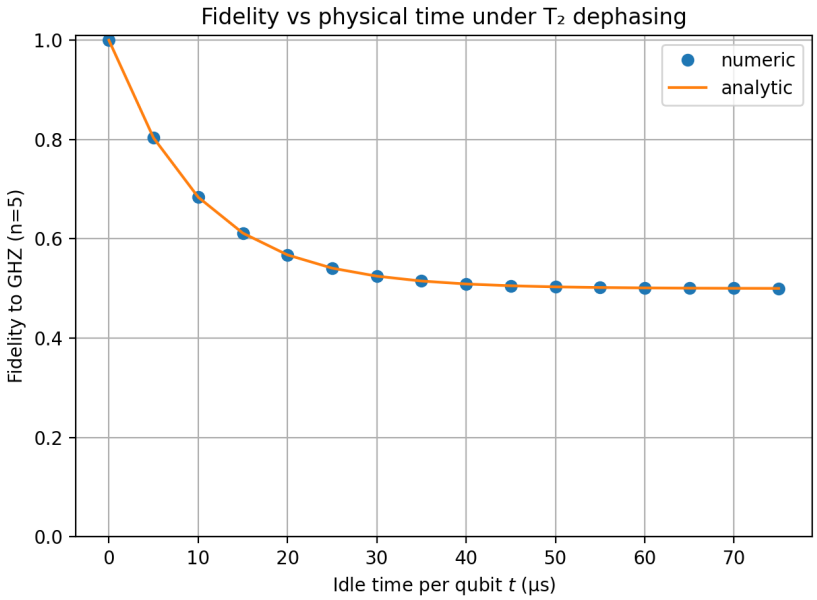

Figure 4.6: Fidelity between the decohered state and the ideal $N = 5$ GHZ state as a function of physical idle time per qubit t, for a pure dephasing process with $T_2 = 50\,\mu s$ and time step $\Delta t = 5\,\mu s$. The markers show the Qiskit simulation with p_{phase} chosen such that $c = e^{-\Delta t/T_2}$ and $\lambda = 1 - c^2$, while the solid line shows the analytic expression $F(t) = \frac{1}{2}\left(1 + e^{-Nt/T_2}\right)$. The two curves are indistinguishable on the scale of the plot.

In this parametrisation, one can read off, for instance, the characteristic time at which a 5-qubit GHZ loses half of its global coherence. The same $\gamma(t)$ can be used to plot the analytic log-negativity $\mathcal{E}_N(t) = \log_2(1 + |\gamma(t)|)$ vs physical time.

4.7 Comparing different noise channels

Finally, I repeat the idle-only GHZ experiment with other single-qubit channels applied to the identity gates:

- amplitude damping, which drives population towards $|0\rangle$;
- single-qubit depolarising noise, which drives states towards the maximally mixed state.

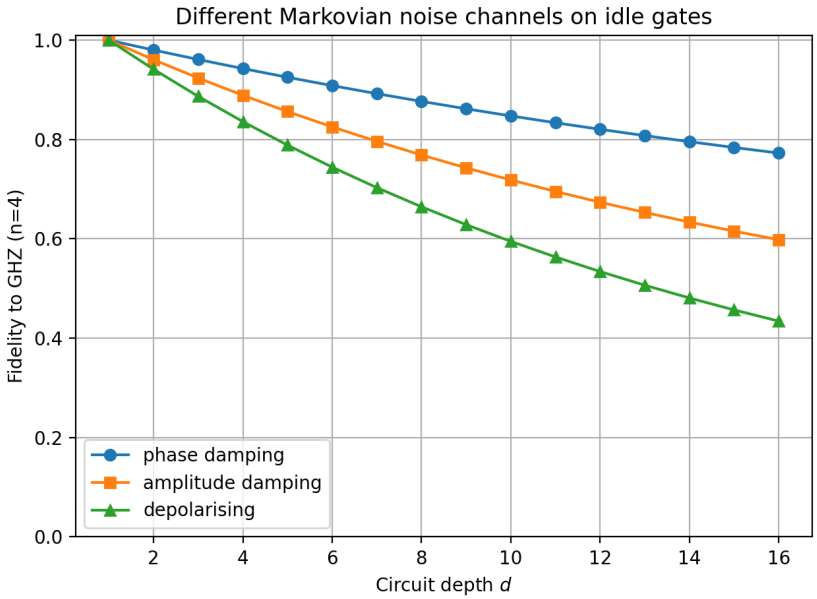

Figure 4.7: GHZ fidelity as a function of circuit depth d for $N = 4$ under three different single-qubit noise channels applied to idle `id` gates: pure phase damping (dephasing), amplitude damping, and single-qubit depolarising noise. All channels use the same nominal error probability $p = 0.02$. Pure dephasing preserves populations and suppresses only coherence, amplitude damping drives the state towards $|0\rangle^{\otimes N}$, and depolarising noise drives it towards the maximally mixed state, leading to distinct fidelity decay profiles for the GHZ state.

At the same nominal error probability, these channels produce distinct fidelity-vs-depth profiles. Pure dephasing preserves populations while suppressing only coherence; amplitude damping gradually shifts population to $|0^{\otimes N}\rangle$, and depolarising noise tends to remove both coherence and population structure. As a result, GHZ fidelity decays in qualitatively different ways across the three channels, illustrating that not all Markovian noise with the same nominal rate has the same impact on multipartite entanglement.

5 Conclusion and limitations

I have investigated how an N-qubit GHZ state degrades under idle-only, memoryless Z-type dephasing using two metrics: (i) state fidelity to the ideal GHZ projector and (ii) logarithmic negativity across the $1|(N-1)$ cut. Across depths up to $d = 16$ and sizes $N \in \{3, 4, 5\}$, both metrics decrease monotonically with circuit depth, with a clear size ordering ($N = 3 > N = 4 > N = 5$ at fixed depth) and a repeats effect (larger r implies faster decay). Within the plotted window and noise levels, fidelity does not visibly approach the $1/2$ floor and $\mathcal{E}_N$ remains above zero, which is consistent with small per-wait dephasing and limited depth.

The analytic dephasing model agrees with the Qiskit density-matrix simulations within numerical precision, and a simple mapping between the phase-damping parameter and a physical T_2 time allows the results to be interpreted in terms of device-level coherence times. A brief comparison with amplitude damping and depolarising noise demonstrates that different Markovian channels can have qualitatively different effects on GHZ robustness.

Several simplifying assumptions limit this study:

- noise acts only during explicit waits (no gate-time noise),
- errors are independent across qubits and time steps (no spatial or temporal correlations),

- the depth and noise levels are modest, so long-time behaviour is not probed.

Future work could relax these assumptions by incorporating gate-time noise, correlated dephasing, more realistic hardware noise models, and active error-mitigation or simple error-correction schemes applied to GHZ-like states.

References

[1] M. A. Nielsen and I. L. Chuang, *Quantum Computation and Quantum Information*, Cambridge University Press (2010).

[2] A. Peres, "Separability Criterion for Density Matrices", Phys. Rev. Lett. **77**, 1413 (1996).

[3] M. Horodecki, P. Horodecki, R. Horodecki, "Separability of Mixed States: Necessary and Sufficient Conditions", Phys. Lett. A **223**, 1–8 (1996).

[4] G. Vidal and R. F. Werner, "Computable measure of entanglement", Phys. Rev. A **65**, 032314 (2002).

[5] Qiskit Aer documentation: phase-damping channel and density-matrix simulation, `https://qiskit.org/ecosystem/aer/`.